

Open-Vocabulary Octree-Graph for 3D Scene Understanding

Zhigang Wang^{1*}, Yifei Su^{2,3*}, Chenhui Li¹, Dong Wang¹, Yan Huang³,
Bin Zhao^{1,4}, Xuelong Li^{1,5†}

¹Shanghai AI Laboratory, ²School of Artificial Intelligence, UCAS, ³MAIS, Institute of Automation,
⁴Northwestern Polytechnical University, ⁵Institute of Artificial Intelligence (TeleAI)

wangzhigang@pjlab.org.cn, suyifei2022@ia.ac.cn

Abstract

Open-vocabulary 3D scene understanding is indispensable for embodied agents. Recent works leverage pre-trained vision-language models (VLMs) for object segmentation and project them to point clouds to build 3D maps. Despite progress, a point cloud is a set of unordered coordinates that requires substantial storage space and does not directly convey occupancy information or spatial relation, making existing methods inefficient for downstream tasks, e.g., path planning and complex text-based object retrieval. To address these issues, we propose **Octree-Graph**, a novel scene representation for open-vocabulary 3D scene understanding. Specifically, a Chronological Group-wise Segment Merging (CGSM) strategy and an Instance Feature Aggregation (IFA) algorithm are first designed to get 3D instances and corresponding semantic features. Subsequently, an adaptive-octree structure is developed that stores semantics and depicts the occupancy of an object adjustably according to its shape. Finally, the Octree-Graph is constructed where each adaptive-octree acts as a graph node, and edges describe the spatial relations among nodes. Extensive experiments on various tasks are conducted on several widely-used datasets, demonstrating the versatility and effectiveness of our method.

1. Introduction

3D scene understanding is receiving increasing attention due to its widespread usage in robots [49] and VR/AR applications [16]. Previous works [18, 20, 31, 35, 39] trained models on particular 3D scene datasets to complete this task. Although significant progress has been achieved, they are limited to a closed-set category. Recently, we have witnessed the impressive generalization ability of foundation models (e.g., SAM [17] and CLIP [30]) which can

*Equal contribution.

†Corresponding author.

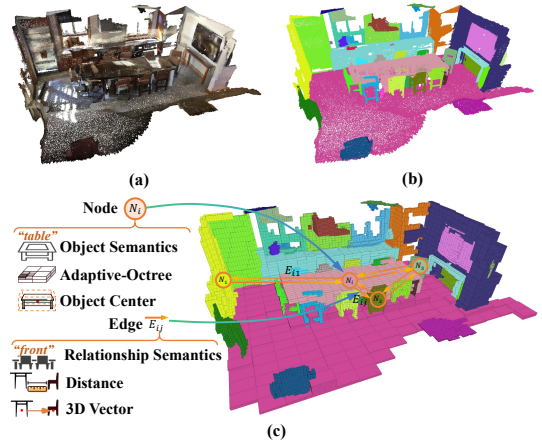


Figure 1. (a) A 3D scene. (b) The corresponding semantic 3D map based on point clouds (6.8M). (c) Our Octree-Graph where each object is represented by the proposed adaptive-octree and each edge contains rich spatial relations among objects. All adaptive-octrees occupy 42KB of storage space in total.

perceive various objects in unseen scenarios, inspiring a lot of open-vocabulary 3D scene understanding methods [3, 4, 6, 15, 24, 41, 46]. Given an RGB-D sequence with camera poses, these methods leverage the off-the-shelf foundation models to generate 2D object masks and corresponding visual-language features and then project them to point clouds to construct a semantic 3D map.

Despite the favorable open-vocabulary understanding capability, they have two drawbacks. 1) **Inefficient space representation of 3D scenes**. Most mainstream methods [14, 28, 45] build the 3D map based on point clouds, as shown in Fig. 1 (b). Point clouds are unordered discrete coordinates that require considerable storage space, making existing methods inefficient to deploy on embodied agents with limited storage resources. Moreover, point clouds lack explicit representation of occupancy information and spatial connectivity which are critical for downstream tasks, e.g., path planning and text-based object retrieval. 2) **Inaccurate semantic object segmentation for 3D map construc-**

tion. Most methods overlook the inaccuracy of foundation models/vision-language models (VLMs) when conducting object segmentation and feature extraction, inevitably causing imprecise 3D object segments and degraded semantics.

To alleviate these problems, we propose **Octree-Graph** as shown in Fig. 1 (c), a novel open-vocabulary scene representation designed to characterize the occupancy and semantics of each object, as well as the relations among them. Specifically, the adaptive-octree is first proposed to depict each object’s occupancy, which inherits the advantages of the octree structure by hierarchically representing a 3D space with structured sub-regions. Compared to the point cloud without regional or hierarchical information, it can save significant storage space. Furthermore, our adaptive-octree initializes each level of sub-regions adaptively according to the shape of an object, enabling precise description of the occupancy within a limited octree depth. This is particularly suitable for objects with large aspect ratios, *e.g.*, walls and floors. Based on this, the Octree-Graph is constructed where each adaptive-octree acts as a graph node, and each edge encompasses rich relations among objects, *e.g.*, distances and relative orientations. The proposed Octree-Graph can be directly applied to downstream tasks such as object retrieval, occupancy queries, and path planning, thereby providing significant convenience.

To obtain accurate semantic objects for Octree-Graph construction, we devise a **training-free** pipeline. First, given input images, 2D proposals are segmented via an off-the-shelf segmenter, and corresponding visual-language features are extracted by pretrained VLMs. Then, they are projected into 3D space as point cloud segments. Second, to correctly merge segments belonging to the same instance, a Chronological Group-wise Segment Merging (CGSM) strategy is proposed where the segments are partitioned into several groups in time order. Each group is individually processed to leverage spatiotemporal details from the neighborhood while avoiding interference from global redundancy. Third, an Instance Feature Aggregation (IFA) method is proposed to obtain semantic representations for each object. Unlike existing works that directly average features as a result, we simultaneously consider the representativeness and distinctiveness of a feature during the fusion process.

Our contributions are summarized as follows.

- We propose the Octree-Graph for open-vocabulary 3D scene understanding, which efficiently depicts objects’ occupancies, semantics, and relations, benefiting several downstream tasks.
- We propose a Chronological Group-wise Segment Merging (CGSM) strategy and an Instance Feature Aggregation (IFA) method to obtain accurate semantic objects.
- We conduct extensive experiments, demonstrating the versatility, effectiveness, and efficiency of our method.

2. Related Work

Foundation Models. Recently, foundation models have exhibited impressive zero-shot perception ability. Here, we review several foundation models related to our work. CLIP [30] is a popular vision-language model that associates images and texts through contrastive learning, significantly promoting many vision-language tasks. SAM [17] is a class-agnostic 2D segmentation model trained with over 1 billion masks, demonstrating powerful zero-shot performance. OVSeg [21] finetunes CLIP to gain the ability of open-vocabulary semantic segmentation. CropFormer [29] fuses the full image and high-resolution image crops to improve segmentation performance. TAP [27] can simultaneously conduct recognition, segmentation, and caption generation. Additionally, many other methods [5, 7, 9, 13, 19, 23, 25, 32, 40, 42, 50] are proposed for 2D open-vocabulary object detection and segmentation.

Open-Vocabulary 3D Scene Understanding. Based on the organization form of scene representation, we categorize these works into three types. 1) **point/grid-wise 3D mapping**. This branch involves directly projecting semantic features to each 3D point. OpenScene [28] extracts CLIP features from the images and densely projects them to the point cloud. ConceptFusion [14] also builds a point-wise map by fusing global and region-level features. VLMaps [11] adopts a similar pipeline to project visual-language features to a grid-based top-down map. 2) **instance-wise 3D mapping**. These works explicitly obtain each individual 3D instance and fuse its visual-language features for 3D mapping. OpenIns3D [12] is a 3D-input-only framework that gets interesting objects by open-vocabulary detection, and then assigns categories to 3D instance proposals. OVIR-3D [24] presents a 2D-to-3D pipeline where 2D masks are projected into 3D space for instance merging based on semantic similarity and 3D overlap. SAM3D [47] and MaskClustering [45] design bottom-up bidirectional merge and view-consensus-guided approaches for better instance merging, respectively. SAI3D [48] uses both 2D proposals and 3D super points, developing a region-growing algorithm for instance segmentation. OpenMask3D [37] and Open3DIS [26] leverage extra 3D instance segmentation models to get more accurate object proposals. However, the used 3D models cannot be considered purely zero-shot methods. 3) **3D scene graph**. A few works use a graph to organize the scene, where each node represents an object and each edge describes inter-object relations [22]. ConceptGraph [6] follows the 2D-to-3D manner, constructing a scene graph to enhance complex spatial reasoning. HOV-SG [41] proposes a hierarchical open-vocabulary 3D scene graph to enable scene representation of different granularities. In contrast, our method can provide more accurate semantic object proposals and more efficient spatial representation.

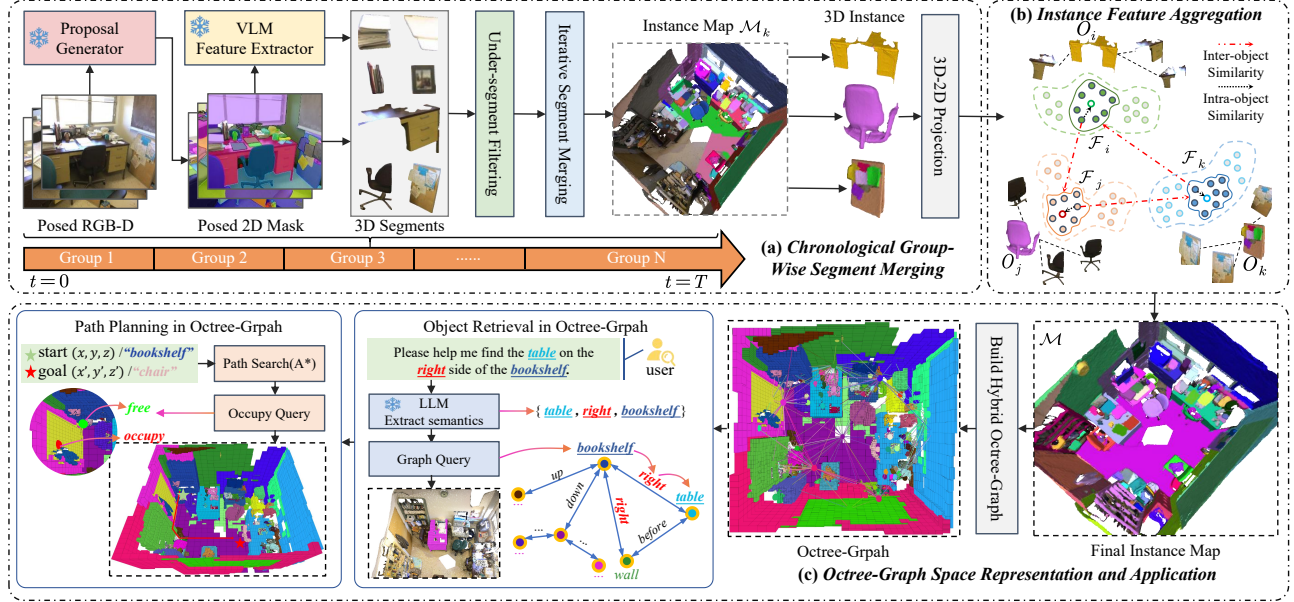


Figure 2. Overview of our Octree-Graph. (a) Chronological Group-wise Segment Merging (CGSM). Given posed RGB-D inputs, 2D masks with semantic features are first extracted and then projected into the 3D space where CGSM is conducted to merge segments. (b) Instance Feature Aggregation (IFA). Feature aggregation is performed for each merged object, which considers both intra- and inter-object similarity. (c) The Octree-Graph is constructed to efficiently and accurately represent the scene, facilitating various downstream tasks.

3. Method

3.1. Framework Overview

As shown in Fig 2, given a sequence of RGB images $\mathcal{I}_c = \{\mathbf{I}_t^c\}_{t=1}^T$ and depth images $\mathcal{I}_d = \{\mathbf{I}_t^d\}_{t=1}^T$ scanned in a scene, we first leverage VLMs to extract segment proposals (§ 3.2). Next, we chronologically merge these segments into an instance map \mathcal{M} via a group-wise merging strategy (§ 3.3). Then we dynamically aggregate the redundant semantics of each instance into a distinctive feature (§ 3.4). Finally, we build an Octree-Graph G to represent spatial relations among instances, with the adaptive-octree to detail instance occupancy. Based on this, we implemented LLM-based object retrieval and path planning algorithms (§ 3.5).

3.2. Segment Proposal and Comprehension

For each frame \mathbf{I}_t^c , we initially adopt an off-the-shelf proposal generator, e.g., CropFormer [29], to extract a set of 2D masks $\mathcal{P}_t^{2d} = \{\mathbf{m}_{t,i}\}_{i=1}^{n_t}$, where n_t is the mask number. We then filter out tiny and marginal masks to ensure the proposal quality. Next, each $\mathbf{m}_{t,i}$ is fed into the visual encoder and caption generator to obtain the visual feature $\mathbf{f}_{t,i}^v$ and caption feature $\mathbf{f}_{t,i}^c$. Finally, we project mask $\mathbf{m}_{t,i}$ into the 3D space as a point cloud segment $\mathcal{S}_{t,i}$ and perform DBSCAN [34] denoise, obtaining segments $\mathcal{P}_t^{3d} = \{\mathcal{S}_{t,i}\}_{i=1}^{n_t}$.

3.3. Chronological Group-wise Segment Merging

Existing segment merging strategies are typically categorized into two types: 1) *frame-wise*, sequentially or hierarchically merges the adjacent frames [6, 24], integrating similar segments efficiently. 2) *graph-wise*, iteratively merges segments across all frames [41, 45], ensuring global optimality via a broader spatiotemporal scope. Despite the progress, we argue that the former solely relying on a single frame can be easily affected by proposal noises, e.g., associating unrelated instances once an under-segment is merged. In contrast, the latter is prone to be distracted by global redundant segments. To this end, we propose a Chronological Group-wise Segment Merging (CGSM) strategy, with semantic-guided under-segment filtering and a dynamic threshold decay strategy.

Chronological Group-wise Split. Given the prior that *an instance often appears in multiple consecutive frames during scanning*, CGSM first splits the frames into multiple groups at interval I in time order, obtaining the segments $\mathcal{G}_i = \{\mathcal{S}_{t,*} \mid t \in [iI, (i+1)I]\}$ for the i^{th} group. In this way, a group can retain the adjacent segments while avoiding interference caused by global redundant segments. Next, based on the groups, we perform iterations of merging to integrate separate segments into an instance map. Concretely, we start by merging \mathcal{G}_0 into an intermediate instance map \mathcal{M}_0 . Subsequently, we iteratively take the union $\{\mathcal{M}_{k-1}, \mathcal{G}_k\}$ as input for the k^{th} merging, until the final instance map \mathcal{M} is constructed. Next, we elaborate on the

details of a single merging step.

Segment Group Merging. For two segments $\{\mathcal{S}_m, \mathcal{S}_n\}$, we define $\phi_{\text{sem}}^v(m, n)$ as the cosine similarity between their visual features, and $\phi_{\text{sem}}^c(m, n)$ the cosine similarity between caption features. Regarding geometric similarity, we compute $\phi_{\text{geo}}^{\text{iou}}(m, n)$ as the intersection over union of two segments. Additionally, we calculate the ratio of \mathcal{S}_n contained within \mathcal{S}_m as $\phi_{\text{geo}}^{\text{ior}}(m, n) = |\mathcal{S}_m \cap \mathcal{S}_n| / |\mathcal{S}_n|$. Intuitively, assuming \mathcal{S}_m is an under-segment containing a correct segment \mathcal{S}_n , $\phi_{\text{geo}}^{\text{ior}}(m, n)$ will be relatively large. Based on these, we can collect all segments contained in \mathcal{S}_m as $\mathcal{C}(\mathcal{S}_m) = \{\mathcal{S}_j \mid \phi_{\text{geo}}^{\text{ior}}(m, j) \geq 0.8\}$. We then consider a segment spatially containing objects with diverse semantics to be under-segmented and filter them out, *i.e.*, $\text{Var}(\{\phi_{\text{sem}}^v(m, j) \mid \mathcal{S}_j \in \mathcal{C}(\mathcal{S}_m)\}) \geq \tau_u$, where $\text{Var}(\cdot)$ is variance. To merge the left segments, we compute an overall similarity $\phi = \phi_{\text{geo}}^{\text{iou}} + \phi_{\text{geo}}^{\text{ior}} + \phi_{\text{sem}}^v + \phi_{\text{sem}}^c$, and iteratively merge segments within \mathcal{G}_i . At each iteration, we merge highly similar segments satisfying $\phi(m, n) \geq \theta_i$. However, simply doing so struggles to merge partially observed segments or over-segments sharing low spatial similarity. To this end, we linearly decay θ_i at each step inspired by [41, 48].

3.4. Instance Feature Aggregation

After obtaining the instance map \mathcal{M} , each 3D instance \mathcal{O}_i is associated with multiple features based on 2D-3D relations. To mitigate the noisy features from partial observation and over-segmentation, we re-project each reconstructed instance onto the corresponding 2D images, obtaining refined semantic features $\mathcal{F}_i = \{\mathbf{f}_{i,j}^v, \mathbf{f}_{i,j}^c \mid \mathbf{m}_j \in \mathcal{O}_i\}$ via VLMs, where $\mathbf{f}_{i,j}^v$ and $\mathbf{f}_{i,j}^c$ are visual and caption features of the newly projected mask \mathbf{m}_j . To aggregate segment features, previous methods either perform averaging [6, 24] or select the dominant feature via DBSCAN [37, 41]. However, they overlook the distinction between various instance features. Hence, we propose a dynamic fusion method for an optimal feature both representative and distinctive as shown in Fig. 2 (b). Specifically, take visual modality for illustration, we first employ the DBSCAN algorithm to retain the major cluster $\mathcal{F}_i^p \subset \mathcal{F}_i$, which filters out imperfect views. Next, we average \mathcal{F}_i^p to a central feature $\bar{\mathbf{f}}_i^v$ for each instance, and the neighboring instances of \mathcal{O}_i is then defined by $\mathcal{N}_i = \{\mathcal{O}_k \mid \cos(\bar{\mathbf{f}}_i^v, \bar{\mathbf{f}}_k^v) \geq \tau_d\}$. Based on this, we aggregate the feature cluster \mathcal{F}_i^p into an optimal \mathbf{f}_i^{v*} via assigning a dynamic fusion weight $a_{i,j}^v$ to each $\mathbf{f}_{i,j}^v$:

$$a_{i,j}^v = \cos(\mathbf{f}_{i,j}^v, \bar{\mathbf{f}}_i^v) - \sum_{\mathcal{O}_k \in \mathcal{N}_i} \cos(\mathbf{f}_{i,j}^v, \bar{\mathbf{f}}_k^v), \quad (1)$$

where $\cos(\cdot)$ denotes cosine similarity, and $a_{i,j}^v$ is normalized via softmax. Intuitively, a feature gets a larger weight if it is closer to its own cluster center and farther from others. The caption feature \mathbf{f}_i^{c*} can be formulated by replacing

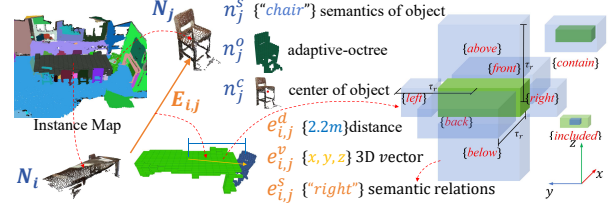


Figure 3. Illustration of the nodes and edges in Octree-Graph.

$\mathbf{f}_{i,j}^v$ with $\mathbf{f}_{i,j}^c$ in the above process. The final instance feature \mathbf{f}_i^* is the sum of \mathbf{f}_i^{v*} and \mathbf{f}_i^{c*} .

3.5. Octree-Graph Construction and Applications

To efficiently and accurately represent a scene, we design a hybrid structure, termed Octree-Graph. This structure utilizes a graph as the high-level architecture to organize objects and their spatial relations. Furthermore, we propose an adaptive-octree to depict the occupancy information of each object, which acts as a node of the Octree-Graph.

Graph Construction. An Octree-Graph can be defined as G with nodes \mathbf{N}_* and edges \mathbf{E}_* . The node \mathbf{N}_i consists of correlated semantics n_i^s (*e.g.*, captions and features), center n_i^c , and adaptive-octree n_i^o . While the edge $\mathbf{E}_{i,j}$ comprises the semantic relation $e_{i,j}^s$, spatial distance $e_{i,j}^d$ and the 3D vector $\mathbf{e}_{i,j}^v$ between node i and node j . Besides, we determine whether to establish an edge between two nodes based on whether their Euclidean distance is below the threshold τ_r . Notably, the semantic relations between nodes are aligned with the world coordinate system of the corresponding point cloud. As shown in Fig. 3, the semantic relation $e_{i,j}^s$ between node \mathbf{N}_i and \mathbf{N}_j is characterized as “right”.

Adaptive-Octree Construction. The classical octree [10] is a tree-based structure capable of efficiently representing 3D space with much less storage requirements than point clouds. During octree construction, the root node is defined by the minimal bounding box containing the point cloud. This box, centered at $c \in \mathbb{R}^3$ with a side length of d , is divided into eight sub-regions of side length $d/2$ using axis-aligned planes. Each sub-region serves as a child node, and the process continues recursively for each node until the desired depth L_{max} is reached or no point clouds are present within the node. We recommend referring to [10] for more details about the octree.

However, traditional octrees use cubic voxels to depict occupancy details, leading to dilemmas of redundant representation, *e.g.*, an object with a large aspect ratio requires a very deep octree to approximate its shape. To this end, we propose the adaptive-octree with varying voxels that adaptively adjust their sizes and shapes according to the object’s shape. As shown in Fig. 4, an adaptive-octree is constructed from an instance-level point cloud P , where its bounding box is defined by $\mathbf{b}_{\text{min}} = \{\min(P_x), \min(P_y), \min(P_z)\}$ and $\mathbf{b}_{\text{max}} = \{\max(P_x), \max(P_y), \max(P_z)\}$. Then, the

size and center of each node in this adaptive-octree can be computed as follows:

$$\mathbf{d}_l = ((\mathbf{b}_{\max} + \delta) - (\mathbf{b}_{\min} - \delta)) / 2^l, \quad (2)$$

$$\mathbf{c}_l = \mathbf{c}_{l-1} + \mathbf{d}_l \odot (\Delta_x, \Delta_y, \Delta_z) / 2, \mathbf{c}_0 = (\mathbf{b}_{\min} + \mathbf{b}_{\max}) / 2, \quad (3)$$

where $\mathbf{d}_l = \{d_l^x, d_l^y, d_l^z\}$ is the side lengths of 3 dimensions, \odot means elementwise multiplication. The values of Δ_x , Δ_y , and Δ_z can each be either -1 or 1 , with their combinations indicating the directions from the center of the node to the centers of the eight child nodes. $\mathbf{c}_l \in \mathbb{R}^3$ is the node center, $\delta = 0.01$ is the expansion threshold which ensures that the point cloud located at the boundary is strictly enclosed within the octree. $l \in \{1, 2, \dots, L_{\max}\}$ denotes the depth of the node.

Octree-Graph Applications. Based on the Octree-Graph, we offer object retrieval and path planning functionalities which are critical for embodied agents. For object retrieval, two types of queries are supported, *i.e.*, Query (*target*) and Query (*reference, relation, target*). The former allows for directly locating an object by comparing the similarity between queries and stored semantics. The latter supports complex queries by sequentially locating the reference object, the edge that matches the described relation, and finally the target. For more complex queries, we leverage the reasoning capabilities of LLMs to decompose the task and flexibly call two types of functions to achieve the goal.

In path planning tasks, querying occupancy information is fundamental. The proposed Octree-Graph supports both coarse and fine-grained occupancy querying. Initially, coarse-grained queries are performed within the graph nodes to identify the associated adaptive-octree and its bounding box. Subsequent recursive queries within this adaptive-octree ascertain whether a specific location is occupied. Through the Octree-Graph, we can easily implement path planning algorithms like classical A^* [8].

4. Experiment

To validate the versatility and effectiveness of our method, we carry out extensive experiments, including semantic/instance segmentation, text-based object retrieval, and path planning. We compare our method with different SOTA methods in these tasks, and conduct comprehensive ablation studies to investigate several key designs. More results and analyses can be found in our **supplementary material**.

4.1. Implementation Details

We use CropFormer [29] as the 2D proposal generator following [45]. To extract visual features, we test two commonly used VLMs, *i.e.*, CLIP ViT-H [30] and OVSeg ViT-L [21]. We adopt TAP [27] for generating the mask caption. Additionally, we filtered out masks with pixels less

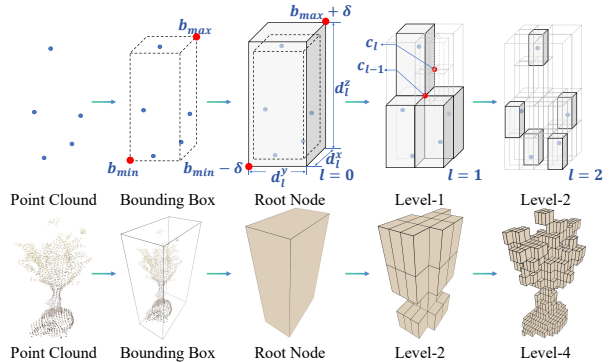


Figure 4. Illustration of the construction of the adaptive-octree. The above displays the process, and the below shows an example.

than 25 and segments with points less than 50. The similarity threshold τ_d and under-segment filtering threshold τ_u are empirically set to 0.7 and 0.01. Considering the dimensions of indoor objects, we set the maximum depth L_{\max} of the adaptive-octree to 4 and establish an edge threshold τ_r of 3 meters within the graph.

4.2. Dataset and Evaluation Metrics

Dataset. For zero-shot 3D semantic segmentation, we evaluate our method on common scenes following [6, 14, 41], *i.e.*, 8 scenes from Replica [36] dataset and 5 scenes from ScanNet [2]. For zero-shot 3D instance segmentation, we assess our method on the widely-used ScanNet200 [33] benchmark, including a validation set of 312 scenes with 200 categories. For text-based object retrieval, we test our method on Sr3D [1] dataset, and follow the experiment setting of BBQ [22] that subsampled 526 free-form queries from 8 scenes. For the path planning task, we employ the HM3DSem [43] dataset used in HOV-SG [41], where 8 scenes are selected for evaluation.

Evaluation Metrics. Following the mainstream evaluation metrics, we assess 3D semantic segmentation results via commonly used mean IoU (mIoU), frequency-weighted mean IoU (F-mIoU), and mean Accuracy (mAcc). For 3D instance segmentation we report the standard Average Precision (AP) at IoU thresholds 25% and 50%, along with the mean of AP from 50% to 95% at 5% interval. For text-based object retrieval, we follow BBQ [22], using Acc@0.1 and Acc@0.25 as evaluation metrics where retrieval is treated as a true positive if the IoU between the predicted object’s bounding box and the ground-truth bounding box surpasses 0.1 and 0.25, respectively. For the path planning task, we randomly select positions in the empty areas of a scene as the starting point and destination, using the A^* [8] algorithm for navigation. When the endpoint of navigation is within a threshold s (*i.e.*, 1m, 0.5m, and 0.25m) from the destination, the path planning is considered successful.

Besides, to quantify spatial representation accuracy, we

Method	CLIP Backbone	Replica			ScanNet		
		mIoU \uparrow	F-mIoU \uparrow	mAcc \uparrow	mIoU \uparrow	F-mIoU \uparrow	mAcc \uparrow
ConceptFusion [14]	OVSeg	0.10	0.21	0.16	0.08	0.11	0.15
	Vit-H-14	0.10	0.18	0.17	0.11	0.12	0.21
ConceptGraph [6]	OVSeg	0.13	0.27	0.21	0.15	0.18	0.23
	Vit-H-14	0.18	0.23	0.30	0.16	0.20	0.28
HOV-SG [41]	OVSeg	0.144	0.255	0.212	0.214	0.258	0.420
	Vit-H-14	0.231	0.386	0.304	0.222	0.303	0.431
Ours	OVSeg	0.320	0.553	0.414	0.393	0.508	0.601
	Vit-H-14	0.263	0.479	0.387	0.356	0.477	0.574

Table 1. Zero-shot 3D semantic segmentation results on Replica and ScanNet benchmark.

Method	AP \uparrow	AP50 \uparrow	AP25 \uparrow
<i>sup. mask + sup. semantic</i>			
Mask3D [35]	26.9	36.2	41.4
<i>sup. mask + z.s. semantic</i>			
Open3DIS [26]	23.7	29.4	32.8
Open3DIS [26] (3D only)	18.6	23.1	27.3
OpenMask3D [37] (Mask3D)	15.4	19.9	23.1
Ours (Mask3D)	23.2	30.3	33.3
<i>z.s. mask + z.s. semantic</i>			
OVIR-3D [24]	9.3	18.7	25.0
SAM3D [47]	9.8	15.2	20.7
SAI3D [48]	12.7	18.8	24.1
Mask-Clustering [45]	12.0	23.3	30.1
Ours	14.3	25.8	33.6

Table 2. 3D instance segmentation results on ScanNet200. *sup.* means supervised training, *z.s.* denotes the zero-shot setting.

Method	Retrieval Algorithm	Acc \uparrow @0.1	Acc \uparrow @0.25
ConceptGraphs [6]	<i>Deductive</i> [22]	0.15	0.08
Open-Fusion [44]	CLIP [30]	0.13	0.02
BBQ [22]	CLIP [30]	0.10	0.06
BBQ [22]	<i>Deductive</i> [22]	0.23	0.18
Ours	Octree-Graph+LLM	0.26	0.23

Table 3. Text-based object retrieval results on the Sr3D dataset.

introduce the Effective Occupancy Ratio (EOR) as a metric. The occupancy range O_{pc} of a point cloud is determined by expanding this point cloud with a dilation $\Delta r = 0.005$, and the occupancy range of the octree is denoted as O_{oct} . Then, the EOR is calculated as $EOR = \frac{O_{oct} \cap O_{pc}}{O_{oct}}$. We denote the mean EOR for all objects in a scene as mEOR.

Method	SR($s=1.0m$)	SR($s=0.5m$)	SR($s=0.25m$)
HOV-SG [41]	55.25	46.75	32.16
Ours	97.88	96.88	96.38

Table 4. Path planning results on HM3DSem. SR denotes success rate (%). s is the threshold within which the distance between the navigation endpoint and the destination is considered successful.

4.3. Quantitative Comparison

3D Semantic Segmentation. Tab. 1 reports the numerical results for zero-shot 3D semantic segmentation on Replica and ScanNet datasets. In this experiment, we compare the results generated by our CGSM and IFA with other works. It can be seen that our method significantly outperforms existing methods across all metrics on both datasets, demonstrating the effectiveness of the proposed CGSM and IFA. Compared to the existing SoTA 3D scene graph, HOV-SG [41], we achieve **+8.9%** mIoU and **+11.0%** mAcc on the Replica dataset. Similarly, we present a **+17.1%** mIoU and a **+17.0%** mAcc on ScanNet with the same settings.

3D Instance Segmentation. The quantitative results for 3D instance segmentation are shown in Tab. 2. We follow [45] to categorize all methods into 3 groups based on whether the proposal generation and semantic prediction are trained. Under the fully zero-shot setting, our method surpasses the previous most advanced method with gains of **2.3%**, **2.5%**, and **3.5%** in AP, AP25 and AP50, respectively. These results further demonstrate the effectiveness of the proposed CGSM and IFA. When using supervised 3D models for proposal generation, our method significantly outperforms OpenMask3D [37] and the Open3DIS [26] variant with only the 3D proposals, validating the superiority of our feature aggregation method IFA. Besides, our method achieves comparable results with the corresponding SOTA method Open3DIS [26], which specially designs a combination of 2D and 3D proposals.

Merging Strategy	mIoU \uparrow	F-mIoU \uparrow	mAcc \uparrow
Frame-wise	0.323	0.439	0.519
Global-wise	0.286	0.414	0.476
Ours (CGSM) $I=400$	0.338	0.463	0.555
Ours (CGSM) $I=200$	0.356	0.477	0.574
Ours (CGSM) $I=100$	0.344	0.462	0.571

Table 5. Ablation study on the segment merging strategy and different temporal intervals for group partitioning of our CGSM.

under-segment filtering	threshold decay	mIoU \uparrow	F-IoU \uparrow	mAcc \uparrow
\times	\times	0.337	0.460	0.547
\checkmark	\times	0.346	0.471	0.557
\checkmark	\checkmark	0.356	0.477	0.574

Table 6. Ablations study on the strategies for segment merging.

Aggregation Strategy	mIoU \uparrow	F-mIoU \uparrow	mAcc \uparrow
Average	0.338	0.453	0.563
Top-5	0.342	0.470	0.570
DBSCAN	0.345	0.459	0.566
Ours (IFA)	0.356	0.477	0.574

Table 7. Ablation study on various feature aggregation strategies.

Text-based Object Retrieval. Tab. 3 presents the comparison results of text-based object retrieval on Sr3D [1] dataset. Our method outperforms the SOTA method BBQ [22] by **3.0%** and **5.0%** in terms of Acc@0.1 and Acc@0.25, respectively. We attribute the performance gain to our accurate semantic object segmentation and the rich relations stored in the Octree-Graph.

Path Planning. For each sense in the HM3DSem [43] dataset, we randomly select 100 pairs of starting points and destinations in navigable areas. HOV-SG [41] can be directly used for path planning, so it is evaluated and compared with our method in this task. Tab. 4 shows the results, we can see that our method significantly surpasses HOV-SG, especially when the threshold s is small. This is because HOV-SG relies on Voronoi graph [38] for path planning where the waypoints and paths are pre-calculated, making it improper for precise navigation. In contrast, our Octree-Graph supports navigation to any empty area, unless the destination is mistakenly occupied by the adaptive-octree.

4.4. Ablation Studies

We analyze the impact of our key designs via zero-shot semantic segmentation experiments on ScanNet.

Effect of Group-Wise Split. We compare the proposed Chronological Group-wise Segment Merging (CGSM) with

Method	Replica		ScanNet	
	Size \downarrow	mEOR \uparrow	Size \downarrow	mEOR \uparrow
Point cloud	18.5MB		6.4MB	
Octree	17.6KB	0.0057	41.1KB	0.0041
Adaptive-octree	29.8KB	0.0108	69.3KB	0.0070

Table 8. Ablation study on the efficiency of the adaptive-octree.

the vanilla frame-wise and global-wise merging strategies. As shown in Tab. 5, we achieve notable gains compared to both methods, with **+3.3%** mIoU over frame-wise merging and **+7.0%** mIoU over global-wise merging. We attribute this to the group-wise merging’s ability to concentrate on the segment adjacency while avoiding global redundancy. We also analyze the impact of hyper-parameter I , and the results in Rows 2-4 show that our method exhibits robustness to I ranging from 100 to 400.

Analysis of Designs on Segment Merging. Tab. 6 presents the results with two key components for merging a single group. Row 0 serves as a fixed-threshold group-wise merging baseline with no extra design. Row 1 is equipped with our semantic-guided under-segment filtering, and achieves **+0.9%** mIoU and **+1.0%** mAcc. Row 2 further incorporates the threshold decay strategy, resulting in an additional **1.0%** mIoU and **1.7%** mAcc gains. These validate the effectiveness of the two strategies during each group-wise merging.

Effect of Instance Feature Aggregation. In Tab. 7, we compare the proposed Instance Feature Aggregation (IFA) method with several commonly used methods. Row 1 simply averages features across all views, yielding unsatisfactory results. Row 2 and Row 3 leverage Top-5 criterion [35, 37] and DBSCAN algorithm [41] to select the predominant feature, achieving gains of **+0.4%** and **+0.7%** mIoU, respectively. By contrast, our IFA achieves an improvement of **1.8%** mIoU over Row 1. This is because we additionally incorporate the inter-object feature differences while keeping the intra-object consistency during aggregation.

Occupancy Representation Efficiency. Based on the results of instance generation in Replica and ScanNet, Tab. 8 provides a comparison of different spatial representations with respect to storage space and the accuracy of occupancy representation. For the same scene, octree and the proposed adaptive-octree consume two orders of magnitude less storage space compared to point clouds. The proposed adaptive-octree structure requires a bit more storage than the traditional octree due to its additional record of bounding boxes for each object. However, at the same depth, the adaptive-octree exhibits a much higher mEOR compared to the octree. This means that the space described by the adaptive-octree is more closely aligned with the regions of the target point cloud distribution. In summary, the adaptive-octree structure requires much less storage space

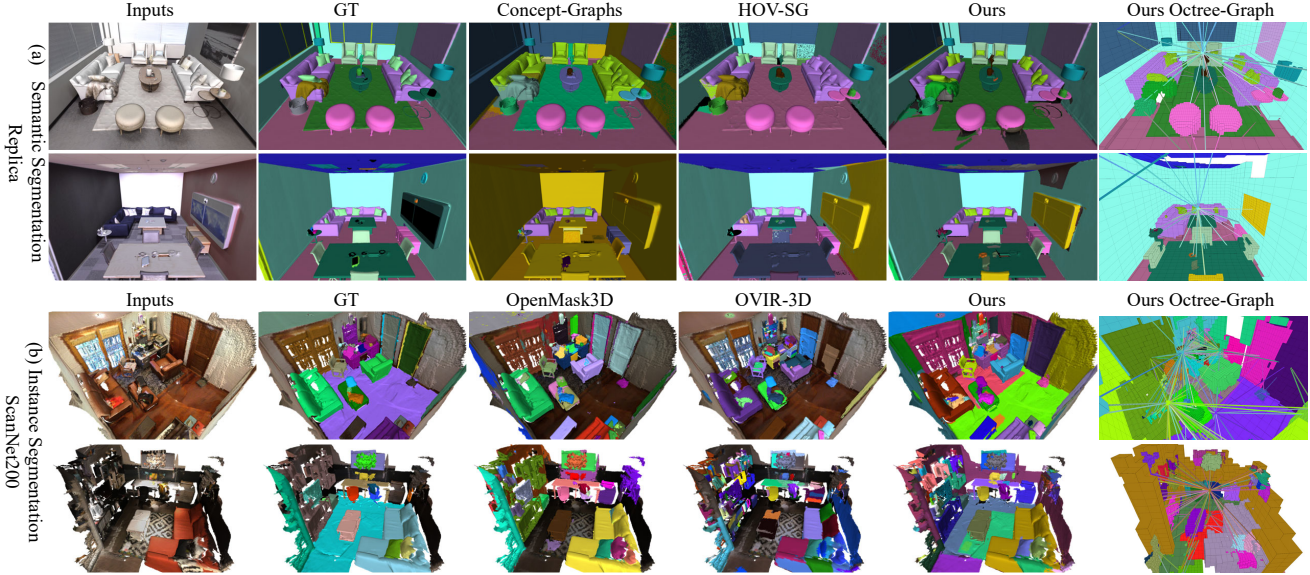


Figure 5. Visual comparisons. (a) Semantic segmentation results on Replica. (b) Instance segmentation results on ScanNet200.

than point clouds and provides more accurate occupancy information than a traditional octree.

4.5. Qualitative Analysis

Visualization Results. Fig. 5 visualizes the results of semantic segmentation and instance segmentation, respectively. We can see that our method exhibits more accurate object semantics and fewer incorrect segments than comparison methods. Fig. 7 demonstrates the segment merging results of our CGSM and its baseline (*i.e.*, frame-wise sequential merging), where CGSM correctly resolves the over-segmented long table without introducing excessive merges between different objects.

Object retrieval and Path planning. Fig. 6 presents object retrievals which are first processed to extract key semantic information using an LLM. After that, the query functions of the Octree-Graph are employed to locate an object. As shown in Fig. 6 (a), queries that solely focus on a target retrieve all objects in the scene that match the query. By incorporating additional spatial constraints, the search can be further refined to locate the desired target accurately.

Fig. 6 (b) illustrates the path planning via our Octree-Graph. As shown in the upper part, a coarse-grained occupancy query at the node level results in a navigation path circumventing obstacles. When further utilizing the fine-grained occupancy querying capability of the adaptive-octree, some small navigable spaces are discovered, enabling small robots to pass underneath tables and chairs.

5. Conclusion

In this paper, we propose Octree-Graph, a novel scene representation for open-vocabulary 3D scene understanding.

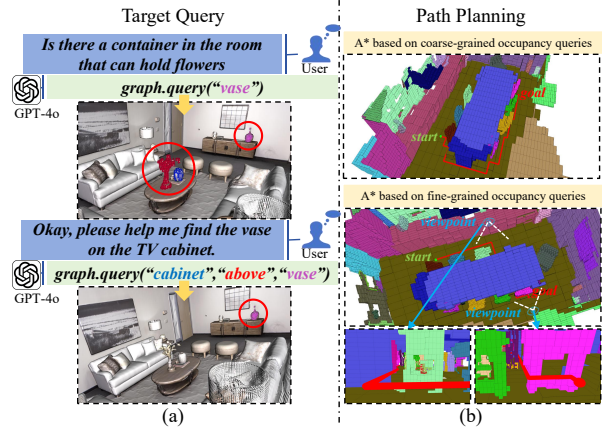


Figure 6. (a) Object retrieval in Octree-Graph through an LLM. (b) Path planning through A* algorithm.

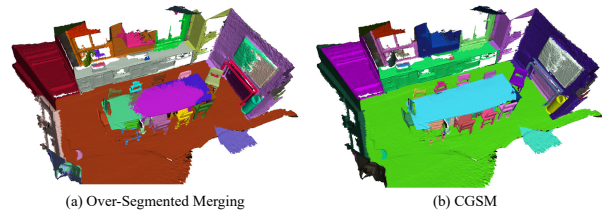


Figure 7. Segment merging comparison between the baseline and our CGSM.

Specifically, an adaptive-octree structure is devised to characterize the occupancy of an object, which acts as the node of the Octree-Graph. The edges describe rich relations among objects for spatial reasoning. For Octree-Graph construction, we also develop a training-free pipeline to con-

duct semantic object segmentation, where a Chronological Group-wise Segment Merging (CGSM) strategy is designed to alleviate inaccurate segment proposals, and an Instance Feature Aggregation (IFA) method is devised to get a semantic feature both representative and distinctive. Extensive evaluations on several tasks validate the versatility and effectiveness of our Octree-Graph.

References

- [1] Panos Achlioptas, Ahmed Abdelreheem, Fei Xia, Mohamed Elhoseiny, and Leonidas J. Guibas. Referit3d: Neural listeners for fine-grained 3d object identification in real-world scenes. In *Computer Vision - ECCV 2020 - 16th European Conference, Glasgow, UK, August 23-28, 2020, Proceedings, Part I*, pages 422–440, 2020. [5](#), [7](#)
- [2] Angela Dai, Angel X Chang, Manolis Savva, Maciej Halber, Thomas Funkhouser, and Matthias Nießner. Scannet: Richly-annotated 3d reconstructions of indoor scenes. In *Proceedings of the IEEE Conference on Computer Vision and Pattern Recognition*, pages 5828–5839, 2017. [5](#)
- [3] Runyu Ding, Jihan Yang, Chuhui Xue, Wenqing Zhang, Song Bai, and Xiaojuan Qi. Lowis3d: Language-driven open-world instance-level 3d scene understanding. *CoRR*, abs/2308.00353, 2023. [1](#)
- [4] Runyu Ding, Jihan Yang, Chuhui Xue, Wenqing Zhang, Song Bai, and Xiaojuan Qi. Pla: Language-driven open-vocabulary 3d scene understanding. In *Proceedings of the IEEE/CVF Conference on Computer Vision and Pattern Recognition*, 2023. [1](#)
- [5] Golnaz Ghiasi, Xiuye Gu, Yin Cui, and Tsung-Yi Lin. Scaling open-vocabulary image segmentation with image-level labels. In *Computer Vision - ECCV 2022 - 17th European Conference, Tel Aviv, Israel, October 23-27, 2022, Proceedings, Part XXXVI*, pages 540–557, 2022. [2](#)
- [6] Qiao Gu, Alihusein Kuwajerwala, Sacha Morin, Krishna Murthy Jatavallabhula, Bipasha Sen, Aditya Agarwal, Corban Rivera, William Paul, Kirsty Ellis, Rama Chellappa, et al. Conceptgraphs: Open-vocabulary 3d scene graphs for perception and planning. *arXiv preprint arXiv:2309.16650*, 2023. [1](#), [2](#), [3](#), [4](#), [5](#), [6](#)
- [7] Xiuye Gu, Tsung-Yi Lin, Weicheng Kuo, and Yin Cui. Open-vocabulary object detection via vision and language knowledge distillation. In *The Tenth International Conference on Learning Representations, ICLR 2022, Virtual Event, April 25-29, 2022*, 2022. [2](#)
- [8] Peter E Hart, Nils J Nilsson, and Bertram Raphael. A formal basis for the heuristic determination of minimum cost paths. *IEEE transactions on Systems Science and Cybernetics*, 4(2):100–107, 1968. [5](#)
- [9] Shuting He, Henghui Ding, and Wei Jiang. Semantic-promoted debiasing and background disambiguation for zero-shot instance segmentation. In *IEEE/CVF Conference on Computer Vision and Pattern Recognition, CVPR 2023, Vancouver, BC, Canada, June 17-24, 2023*, pages 19498–19507, 2023. [2](#)
- [10] Armin Hornung, Kai M Wurm, Maren Bennewitz, Cyrill Stachniss, and Wolfram Burgard. Octomap: An efficient probabilistic 3d mapping framework based on octrees. *Autonomous robots*, 34:189–206, 2013. [4](#)
- [11] Chenguang Huang, Oier Mees, Andy Zeng, and Wolfram Burgard. Visual language maps for robot navigation. In *IEEE International Conference on Robotics and Automation, ICRA 2023, London, UK, May 29 - June 2, 2023*, pages 10608–10615, 2023. [2](#)
- [12] Zhening Huang, Xiaoyang Wu, Xi Chen, Hengshuang Zhao, Lei Zhu, and Joan Lasenby. Openins3d: Snap and lookup for 3d open-vocabulary instance segmentation. *CoRR*, abs/2309.00616, 2023. [2](#)
- [13] Dat Huynh, Jason Kuen, Zhe Lin, Jiuxiang Gu, and Ehsan Elhamifar. Open-vocabulary instance segmentation via robust cross-modal pseudo-labeling. In *IEEE/CVF Conference on Computer Vision and Pattern Recognition, CVPR 2022, New Orleans, LA, USA, June 18-24, 2022*, pages 7010–7021, 2022. [2](#)
- [14] Krishna Murthy Jatavallabhula, Alihusein Kuwajerwala, Qiao Gu, Mohd Omama, Tao Chen, Shuang Li, Ganesh Iyer, Soroush Saryazdi, Nikhil Keetha, Ayush Tewari, Joshua B. Tenenbaum, Celso Miguel de Melo, Madhava Krishna, Liam Paull, Florian Shkurti, and Antonio Torralba. Conceptfusion: Open-set multimodal 3d mapping. *Robotics: Science and Systems*, 2023. [1](#), [2](#), [5](#), [6](#)
- [15] Li Jiang, Shaoshuai Shi, and Bernt Schiele. Open-vocabulary 3d semantic segmentation with foundation models. In *IEEE/CVF Conference on Computer Vision and Pattern Recognition, CVPR 2024, Seattle, WA, USA, June 16-22, 2024*, pages 21284–21294, 2024. [1](#)
- [16] Justin Kerr, Chung Min Kim, Ken Goldberg, Angjoo Kanazawa, and Matthew Tancik. LERF: language embedded radiance fields. In *IEEE/CVF International Conference on Computer Vision, ICCV 2023, Paris, France, October 1-6, 2023*, pages 19672–19682, 2023. [1](#)
- [17] Alexander Kirillov, Eric Mintun, Nikhila Ravi, Hanzi Mao, Chloe Rolland, Laura Gustafson, Tete Xiao, Spencer Whitehead, Alexander C. Berg, Wan-Yen Lo, Piotr Dollár, and Ross Girshick. Segment anything. *arXiv:2304.02643*, 2023. [1](#), [2](#)
- [18] Xin Kong, Shikun Liu, Marwan Taher, and Andrew J. Davison. vmap: Vectorised object mapping for neural field SLAM. In *IEEE/CVF Conference on Computer Vision and Pattern Recognition, CVPR 2023, Vancouver, BC, Canada, June 17-24, 2023*, pages 952–961, 2023. [1](#)
- [19] Boyi Li, Kilian Q. Weinberger, Serge J. Belongie, Vladlen Koltun, and René Ranftl. Language-driven semantic segmentation. In *The Tenth International Conference on Learning Representations, ICLR 2022, Virtual Event, April 25-29, 2022*, 2022. [2](#)
- [20] Kejie Li, Daniel DeTone, Steven Chen, Minh Vo, Ian Reid, Hamid Rezaatofighi, Chris Sweeney, Julian Straub, and Richard A. Newcombe. O DAM: object detection, association, and mapping using posed RGB video. In *2021 IEEE/CVF International Conference on Computer Vision, ICCV 2021, Montreal, QC, Canada, October 10-17, 2021*, pages 5978–5988, 2021. [1](#)
- [21] Feng Liang, Bichen Wu, Xiaoliang Dai, Kunpeng Li, Yinan Zhao, Hang Zhang, Peizhao Zhang, Peter Vajda, and Diana

- Marculescu. Open-vocabulary semantic segmentation with mask-adapted CLIP. In *IEEE/CVF Conference on Computer Vision and Pattern Recognition, CVPR 2023, Vancouver, BC, Canada, June 17-24, 2023*, pages 7061–7070, 2023. 2, 5
- [22] Sergey Linok, Tatiana Zemskova, Svetlana Ladanova, Roman Titkov, and Dmitry Yudin. Beyond bare queries: Open-vocabulary object retrieval with 3d scene graph. *arXiv preprint arXiv:2406.07113*, 2024. 2, 5, 6, 7
- [23] Shilong Liu, Zhaoyang Zeng, Tianhe Ren, Feng Li, Hao Zhang, Jie Yang, Chunyuan Li, Jianwei Yang, Hang Su, Jun Zhu, et al. Grounding dino: Marrying dino with grounded pre-training for open-set object detection. *arXiv preprint arXiv:2303.05499*, 2023. 2
- [24] Shiyang Lu, Haonan Chang, Eric Pu Jing, Abdeslam Boularias, and Kostas Bekris. Ovir-3d: Open-vocabulary 3d instance retrieval without training on 3d data. In *7th Annual Conference on Robot Learning*, 2023. 1, 2, 3, 4, 6
- [25] Matthias Minderer, Alexey A. Gritsenko, Austin Stone, Maxim Neumann, Dirk Weissenborn, Alexey Dosovitskiy, Aravindh Mahendran, Anurag Arnab, Mostafa Dehghani, Zhuoran Shen, Xiao Wang, Xiaohua Zhai, Thomas Kipf, and Neil Houlsby. Simple open-vocabulary object detection. In *Computer Vision - ECCV 2022 - 17th European Conference, Tel Aviv, Israel, October 23-27, 2022, Proceedings, Part X*, pages 728–755, 2022. 2
- [26] Phuc D. A. Nguyen, Tuan Duc Ngo, Evangelos Kalogerakis, Chuang Gan, Anh Tran, Cuong Pham, and Khoi Nguyen. Open3dis: Open-vocabulary 3d instance segmentation with 2d mask guidance. In *Proceedings of the IEEE/CVF Conference on Computer Vision and Pattern Recognition (CVPR)*, 2024. 2, 6
- [27] Ting Pan, Lulu Tang, Xinlong Wang, and Shiguang Shan. Tokenize anything via prompting. *arXiv preprint arXiv:2312.09128*, 2023. 2, 5
- [28] Songyou Peng, Kyle Genova, Chiyu Max Jiang, Andrea Tagliasacchi, Marc Pollefeys, and Thomas A. Funkhouser. Openscene: 3d scene understanding with open vocabularies. In *IEEE/CVF Conference on Computer Vision and Pattern Recognition, CVPR 2023, Vancouver, BC, Canada, June 17-24, 2023*, pages 815–824, 2023. 1, 2
- [29] Lu Qi, Jason Kuen, Tiancheng Shen, Jiuxiang Gu, Wenbo Li, Weidong Guo, Jiaya Jia, Zhe Lin, and Ming-Hsuan Yang. High quality entity segmentation. In *IEEE/CVF International Conference on Computer Vision, ICCV 2023, Paris, France, October 1-6, 2023*, pages 4024–4033, 2023. 2, 3, 5
- [30] Alec Radford, Jong Wook Kim, Chris Hallacy, Aditya Ramesh, Gabriel Goh, Sandhini Agarwal, Girish Sastry, Amanda Askell, Pamela Mishkin, Jack Clark, Gretchen Krueger, and Ilya Sutskever. Learning transferable visual models from natural language supervision. In *Proceedings of the 38th International Conference on Machine Learning, ICML*, pages 8748–8763, 2021. 1, 2, 5, 6
- [31] Damien Robert, Bruno Vallet, and Loïc Landrieu. Learning multi-view aggregation in the wild for large-scale 3d semantic segmentation. In *IEEE/CVF Conference on Computer Vision and Pattern Recognition, CVPR 2022, New Orleans, LA, USA, June 18-24, 2022*, pages 5565–5574. 1
- [32] Dávid Rozenberszki, Or Litany, and Angela Dai. Language-grounded indoor 3d semantic segmentation in the wild. In *Computer Vision - ECCV 2022 - 17th European Conference, Tel Aviv, Israel, October 23-27, 2022, Proceedings, Part XXXIII*, pages 125–141, 2022. 2
- [33] David Rozenberszki, Or Litany, and Angela Dai. Language-grounded indoor 3d semantic segmentation in the wild. In *European Conference on Computer Vision*, pages 125–141. Springer, 2022. 5
- [34] Erich Schubert, Jörg Sander, Martin Ester, Hans-Peter Kriegel, and Xiaowei Xu. DBSCAN revisited, revisited: Why and how you should (still) use DBSCAN. *ACM Trans. Database Syst.*, 42(3):19:1–19:21, 2017. 3
- [35] Jonas Schult, Francis Engelmann, Alexander Hermans, Or Litany, Siyu Tang, and Bastian Leibe. Mask3D: Mask Transformer for 3D Semantic Instance Segmentation. 2023. 1, 6, 7
- [36] Julian Straub, Thomas Whelan, Lingni Ma, Yufan Chen, Erik Wijmans, Simon Green, Jakob J Engel, Raul Mur-Artal, Carl Ren, Shobhit Verma, et al. The replica dataset: A digital replica of indoor spaces. *arXiv preprint arXiv:1906.05797*, 2019. 5
- [37] Ayça Takmaz, Elisabetta Fedele, Robert W. Sumner, Marc Pollefeys, Federico Tombari, and Francis Engelmann. Open-Mask3D: Open-Vocabulary 3D Instance Segmentation. In *Advances in Neural Information Processing Systems*, 2023. 2, 4, 6, 7
- [38] Sebastian Thrun and Arno Bücken. Integrating grid-based and topological maps for mobile robot navigation. In *Proceedings of the Thirteenth National Conference on Artificial Intelligence and Eighth Innovative Applications of Artificial Intelligence Conference, AAAI 96, IAAI 96, Portland, Oregon, USA, August 4-8, 1996, Volume 2*, pages 944–950, 1996. 7
- [39] Khoi Nguyen Tuan Duc Ngo, Binh-Son Hua. Isbnet: a 3d point cloud instance segmentation network with instance-aware sampling and box-aware dynamic convolution. In *Proceedings of the IEEE/CVF Conference on Computer Vision and Pattern Recognition (CVPR)*, 2023. 1
- [40] Vibashan VS, Ning Yu, Chen Xing, Can Qin, Mingfei Gao, Juan Carlos Niebles, Vishal M. Patel, and Ran Xu. Mask-free OVIS: open-vocabulary instance segmentation without manual mask annotations. In *IEEE/CVF Conference on Computer Vision and Pattern Recognition, CVPR 2023, Vancouver, BC, Canada, June 17-24, 2023*, pages 23539–23549, 2023. 2
- [41] Abdelrhman Werby, Chenguang Huang, Martin Büchner, Abhinav Valada, and Wolfram Burgard. Hierarchical open-vocabulary 3d scene graphs for language-grounded robot navigation. *Robotics: Science and Systems*, 2024. 1, 2, 3, 4, 5, 6, 7
- [42] Jiarui Xu, Shalini De Mello, Sifei Liu, Wonmin Byeon, Thomas M. Breuel, Jan Kautz, and Xiaolong Wang. Groupvit: Semantic segmentation emerges from text supervision. In *IEEE/CVF Conference on Computer Vision and Pattern Recognition, CVPR 2022, New Orleans, LA, USA, June 18-24, 2022*, pages 18113–18123, 2022. 2

- [43] Karmesh Yadav, Ram Ramrakhya, Santhosh Kumar Ramakrishnan, Théophile Gervet, John M. Turner, Aaron Gokaslan, Noah Maestre, Angel Xuan Chang, Dhruv Batra, Manolis Savva, Alexander William Clegg, and Devendra Singh Chaplot. Habitat-matterport 3d semantics dataset. In *IEEE/CVF Conference on Computer Vision and Pattern Recognition, CVPR 2023, Vancouver, BC, Canada, June 17-24, 2023*, pages 4927–4936, 2023. [5](#), [7](#)
- [44] Kashu Yamazaki, Taisei Hanyu, Khoa Vo, Thang Pham, Minh Tran, Gianfranco Doretto, Anh Nguyen, and Ngan Le. Open-fusion: Real-time open-vocabulary 3d mapping and queryable scene representation. In *2024 IEEE International Conference on Robotics and Automation (ICRA)*, pages 9411–9417. IEEE, 2024. [6](#)
- [45] Mi Yan, Jiazhao Zhang, Yan Zhu, and He Wang. Maskclustering: View consensus based mask graph clustering for open-vocabulary 3d instance segmentation. In *Proceedings of the IEEE/CVF Conference on Computer Vision and Pattern Recognition*, pages 28274–28284, 2024. [1](#), [2](#), [3](#), [5](#), [6](#)
- [46] Jihan Yang, Runyu Ding, Weipeng Deng, Zhe Wang, and Xiaojuan Qi. Regionplc: Regional point-language contrastive learning for open-world 3d scene understanding. In *Proceedings of the IEEE/CVF Conference on Computer Vision and Pattern Recognition*, 2024. [1](#)
- [47] Yunhan Yang, Xiaoyang Wu, Tong He, Hengshuang Zhao, and Xihui Liu. Sam3d: Segment anything in 3d scenes. *arXiv preprint arXiv:2306.03908*, 2023. [2](#), [6](#)
- [48] Yingda Yin, Yuzheng Liu, Yang Xiao, Daniel Cohen-Or, Jingwei Huang, and Baoquan Chen. Sai3d: Segment any instance in 3d scenes. In *Proceedings of the IEEE/CVF Conference on Computer Vision and Pattern Recognition*, pages 3292–3302, 2024. [2](#), [4](#), [6](#)
- [49] Jiazhao Zhang, Liu Dai, Fanpeng Meng, Qingnan Fan, Xuelin Chen, Kai Xu, and He Wang. 3d-aware object goal navigation via simultaneous exploration and identification. In *IEEE/CVF Conference on Computer Vision and Pattern Recognition, CVPR 2023, Vancouver, BC, Canada, June 17-24, 2023*, pages 6672–6682, 2023. [1](#)
- [50] Xingyi Zhou, Rohit Girdhar, Armand Joulin, Philipp Krähenbühl, and Ishan Misra. Detecting twenty-thousand classes using image-level supervision. In *Computer Vision - ECCV 2022 - 17th European Conference, Tel Aviv, Israel, October 23-27, 2022, Proceedings, Part IX*, pages 350–368, 2022. [2](#)